Finite element modeling of auxetic warp knitted fabric made of reentrant geometry

Shuaiquan Zhao, Yu Chen, Yuping Chang, Hong Hu *

Institute of Textiles and Clothing, The Hong Kong Polytechnic University, Hong Kong, China

* Corresponding author, email address: hu.hong@polyu.edu.hk

Abstract

Auxetic fabrics are those with negative Poisson's ratio and have received increasing attention in recent years. In our previous study, a series of auxetic warp knitted fabrics were developed based on reentrant geometry and their auxetic effects were experimentally investigated. Unlike weft knitted fabrics, the preparation and production process of warp knitted fabrics are very complicated and time consuming. However, finite element method can offer an efficient way to simulate and predict their auxetic behavior without performing the manufacturing process and experimental tests. This work aimed to conduct a finite element study of auxetic warp knitted fabric structure. The finite element models were established from the geometry of a real fabric and compared with the experimental results. The study showed that the variation trends of Poisson's ratio agreed well between the simulation and experiment. Although simulation results are slightly different from the experimental ones, it still proves feasible for predicting auxetic effects of auxetic fabrics using the finite element models.

It is expected that this research can offer a useful method to model and simulate the deformation behavior of auxetic warp knitted fabrics, and work as a guide for the design and development of more novel auxetic fabric structures.

Keywords: Auxetic fabric, warp knitting, finite element simulation, deformation behavior

Introduction

Auxetic fabrics are those with negative Poisson's ratio [1, 2]. When stretched, they will expand in lateral direction [3]. This counterintuitive behavior provides them with excellent formability under out of plane bending and enhanced permeability under extension, which makes them very attractive in applications like functional clothing, sportswear, medical textiles, smart filters, etc.[4]. This unusual behavior has also motivated various researchers to develop different types of auxetic fabrics [2, 5]. Up to date, auxetic fabrics which have been developed can be roughly divided into auxetic woven fabrics [6-12], auxetic knitted fabrics [1, 13-18], auxetic nonwoven fabrics [19-21] and special auxetic fabric structures [22].

Compared with other type of fabric forming technologies, weft knitting is the most flexible and effective one [13]. A number of auxetic fabrics have been fabricated using this technology. Liu et al. [23] firstly developed a type of auxetic weft knitted fabrics based on three dimensional structures formed by parallelogram planes, in which purl structure composed of face and reverse loops was arranged into a zigzag shape, and auxetic behavior of the structure was achieved after knitting due to the disequilibrium

of face and reverse loops. They found that all weft knitted fabrics made of this type of structure showed negative Poisson's ratio in both course and wale directions and the experimental results of Poisson's ratio as a function of tensile strain had the same variation trends with the theoretical predictions. They also found that opening angle at initial state is the main factor that influenced auxetic effect of the fabrics. Their research demonstrated that auxetic fabrics could be realized by weft knitting technology. Later, the same research group continued to develop another three auxetic weft knitted fabric structures based on foldable structure, rotating rectangle and reentrant hexagon respectively [13]. All the fabrics achieved auxetic effects but their auxetic effects showed different variation trends with the increase of tensile strain. While the auxetic effect of the fabric based on foldable geometry firstly increased and then decreased with the increase of tensile strains, the auxetic effect of other two fabrics showed decrease trends with the elongation of the fabric. Inspired from the above pioneering works, other researchers also proposed several auxetic weft knitted fabrics [24-26].

Although the preparation and production process are less flexible than weft knitting technology, warp knitting technology has also been used for fabricating auxetic fabrics. The most important advantage of warp knitting lies in its high ability to fabricate net-like structures, which is very useful for producing auxetic geometries. Up to date, various auxetic warp knitted fabrics have been proposed by researchers. Based on reentrant geometry, Ugbolue et al. [27] developed a series of auxetic warp knitted fabrics using conventional yarns. To form the reentrant structure, elastic yarns were inlaid into a ground net warp knitted fabric structure. The inlaid elastic yarns would

shrink after knitting, causing the deformation of the wales to form reentrant structure, thus an auxetic effect was obtained when stretched. Double arrowhead structures can exhibit auxetic effect when they deform under tension, moisture absorption or temperature changes [28]. This structure can be realized using warp knitting technology. Alderson et al. [17] proposed auxetic warp knitted fabrics with different knit patterns based on double arrowhead structure. Some of them achieved auxetic effect along directions at ± 45° to the warp direction. Ma et al. [18, 29] also developed auxetic warp knitted fabrics based on rotational hexagonal structure by using both single needle bar and double needle bar warp knitting machines, respectively. Different from the above researchers, Wang et al. [15] developed 3D auxetic spacer warp knitted fabrics with in-plane negative Poisson's ratio through a post compression and heat setting process, in which conventional hexagonal spacer warp knitted fabrics were firstly compressed along their wale direction to change their non-auxetic geometry to an auxetic geometry. Then the compressed fabrics were subjected to a heat setting process to fix their auxetic geometry. Auxetic fabrics thus developed demonstrated good auxetic effect in both wale direction and course direction. Recently, Zhao et al [14] also developed a series of auxetic warp knitted fabrics based on reentrant geometry. To achieve the expected auxetic geometry, special structures were designed with the use of elastic yarns and stiff yarns. Another type of binding yarn in the front bar was also used to prevent yarn transfer between loops and underlaps. Results showed that the fabrics produced had auxetic effect in both wale direction and course direction. In the wale direction, auxetic effect of the fabrics firstly increased and then decreased with fabric elongation, but the

fabric kept auxetic effect in the whole tensile process till breaking of the fabrics. While in the course direction, auxetic effect decreased with fabric elongation and Poisson's ratio became positive when the tensile strain reached a certain value. Their research also showed that both underlap numbers and diagonal rib length could affect auxetic effect of the fabrics.

Although several auxetic knitted fabrics have been proposed and studied in terms of auxetic behavior and tensile properties, most of the previous works are based on the real auxetic warp knitted fabrics. Compared with experimental studies, finite element analysis is an effective method to predict auxetic behavior of fabrics. The aim of this research is to simulate auxetic behavior of the warp knitted fabric structure developed based on reentrant hexagonal geometry in our previous researches [14, 30] by using finite element method. To establish accurate finite element models, the fabric was first scanned by Leica stereo microscopy system (Leica M125C) to get precise geometry, and then finite element models in both weft and warp directions were established based on the geometry obtained, respectively. The simulation results showed a good agreement with the experimental ones.

Fabric details

The auxetic warp fabric used for building finite element models in this work is shown in Figure 1 (a) and one basic unit of its structure, which is outlined by a red rectangle, is shown in Figure 1 (b). From Figure 1(b), it can be seen that one basic unit is formed

with four diagonal ribs, two vertical ribs, elastic and stiff underlaps. Figure 1(c) illustrates the stitch pattern of the fabric structure.

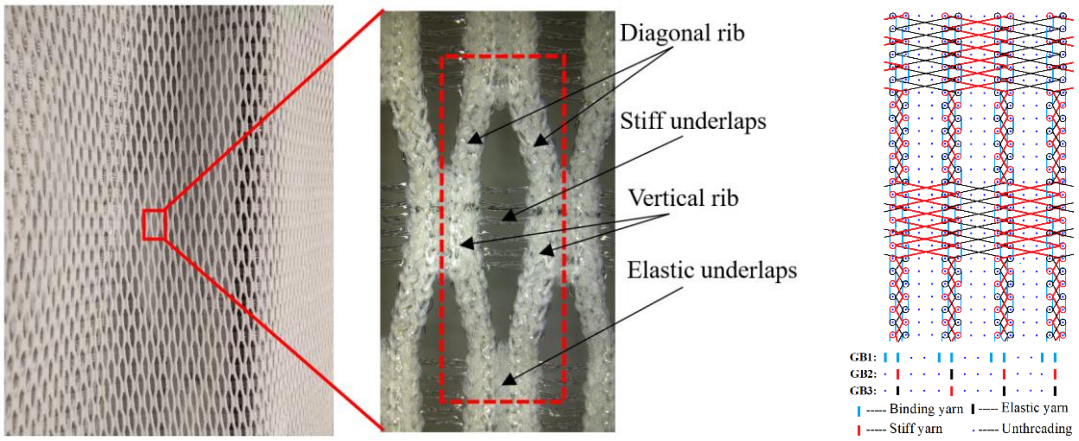

(a) (b) (c)

Figure 1 Auxetic warp knitted fabric used for simulation: (a) overview; (b) one basic unit; (c) stitch pattern.

The fabric was knitted using three types of non-auxetic yarns on a conventional Tricot warp knitting machine. Yarn guide bar settings and yarns used are listed in Table 1. While bar 1 was used to knit chain stitches with binding yarns, bar 2 and bar 3 were used to form the basic reentrant fabric structures. Referred to Figure 2(b), when loaded in the wale direction, the rotation of diagonal ribs will lead to the extension of elastic underlaps and the compression of stiff underlaps at the same time. It should be noted that extension load exerted to the elastic underlaps is equal to the compression load exerted to the stiff underlaps. If the compression load is higher than loading bearing capacity of the stiff underlaps, the stiff underlaps will bend causing the decrease of auxetic effect. Therefore, to get better auxetic effect, stiff yarns should have sufficient

stiffness and elastic yarns should be easily extended. In this work, 0.1mm polyester filament is selected as stiff yarn and 30d polyurethane wrapped by 75d polyester was selected as elastic yarn.

On the other hand, it is well known that warp knitted fabrics are comprised of loops and underlaps. When a load is exerted to a warp knitted fabric structure, yarns transfer between loops and underlaps could take place. If loading is in the wale direction, yarns will transfer from underlaps to wales, causing shrinkage of fabric in the lateral direction. As a result, auxetic effect will be decreased. To enhance the auxetic effect of the fabric, bar 1 was used to form chain stitches which help bind the ground fabric structure to prevent the transfer of yarns between underlaps and loops. Based on the machine gauge, which is 28 needles per inch, the commonly used 75d polyester yarn was selected as binding yarn.

Table 1 Guide bar settings and yarns used

Setting	Yarn
Bar1: (1-0/0-1)*13//(2 in 2 miss)	75d polyester (binding yarn)
Bar2 :(5-6/5-4)*3/ (5-6/1-0)*3/ (5-6/5-4)*4/ (9-10/5-4)*3//(1 in 3 miss)	0.1mm polyester monofilament (stiff yarn), 30d polyurethane wrapped by 75d polyester (elastic yarn)
Bar3: (5-4/5-6)*3/*(5-4/9-10)*3/(5-4/5-6)*4/(1-0/5-6)*3// (1 in 3 miss)	0.1mm polyester monofilament (stiff yarn), 30d polyurethane wrapped by 75d polyester (elastic yarn)

Geometrical model of the fabric structure

After knitting, reentrant geometry of the fabric as shown in Figure 1 was formed. In the previous work [14, 30], auxetic behavior of the fabric was studied under single tensile test and repeating tensile test. It is known that the accuracy of simulation results mainly depends on the geometrical model. To obtain a precise geometry, photos of the fabric were taken by Leica system which can obtain high-quality digital images for measurements as shown in Figure 2 (a). All the photos were taken with 10 times magnification. According to the scale on the photos, measurements of the components in one basic unit can be calculated by screen ruler. Then the photos were inserted into UG 10.0 to obtain outlines of a basic unit with coordinates as shown in Figure 2 (b).

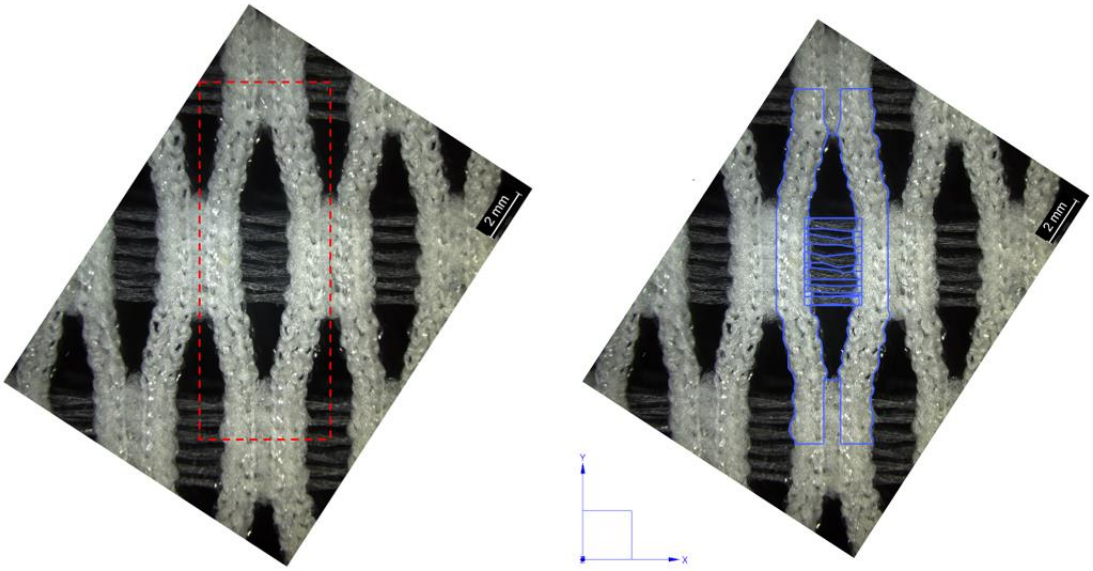

(a) (b)

Figure 2 Photos of the fabric: (a) taken by Leica system; (b) outlined by UG 10.0.

As the number and distribution of elastic underlaps are the same as stiff underlaps, the outlines of stiff underlaps could be used to establish elastic underlaps. Therefore, only stiff underlaps and wales were outlined. After outlining a basic unit of the fabric, the geometrical model of one basic unit was established using UG 10.0 as shown in Figure 3, in which stiff underlaps, wales and elastic underlaps are represented by blue, yellow and red colors, respectively. According to the real fabric dimension, the thickness of the model was set as 0.64 mm.

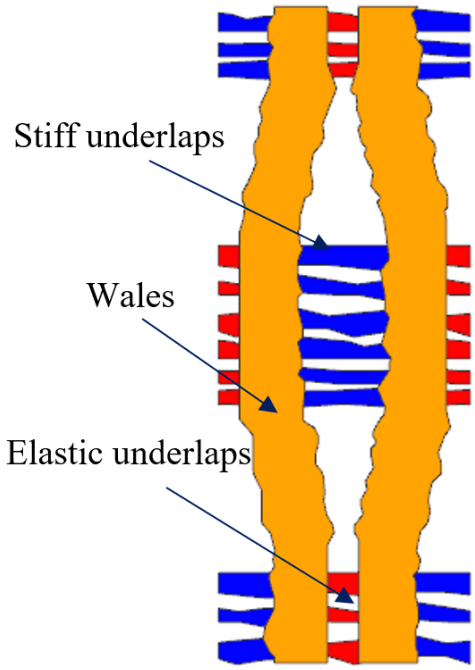

Figure 3 Geometrical model of one basic unit.

Material properties

The basic materials for each component were determined by reference of the experimental results. All the materials were considered as isotropic materials. According to the experimental tests on each component, a bilinear model was proposed

for the stiff underlaps and linear models were suggested for the wales and the elastic underlaps, as shown in Figure 4. By fitting the proposed materials' models with the experimental results, the Young's modulus for each type of component was obtained as 2496.5Mpa and 990.0MPa for stiff underlaps, 0.5MPa for the elastic underlaps, and 30.5MPa for the wales. Regarding the Poisson's ratio, the values used for the stiff underlaps, elastic underlaps and wales were 0.33, 0.45 and 0.35, respectively. The density for all the components was set as 1200kg/m^3 in this study.

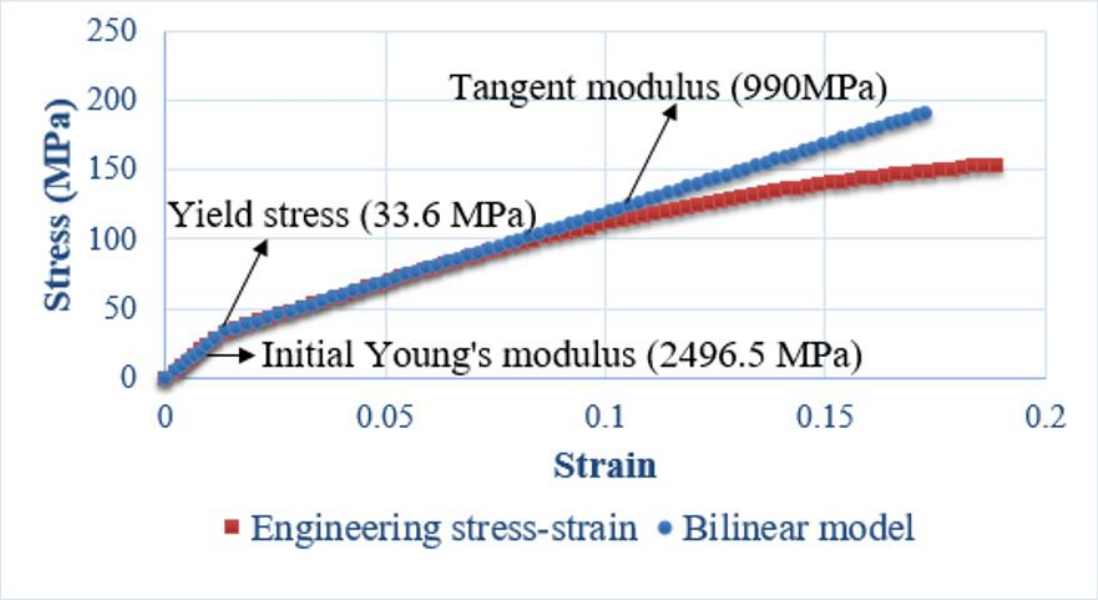

(a)

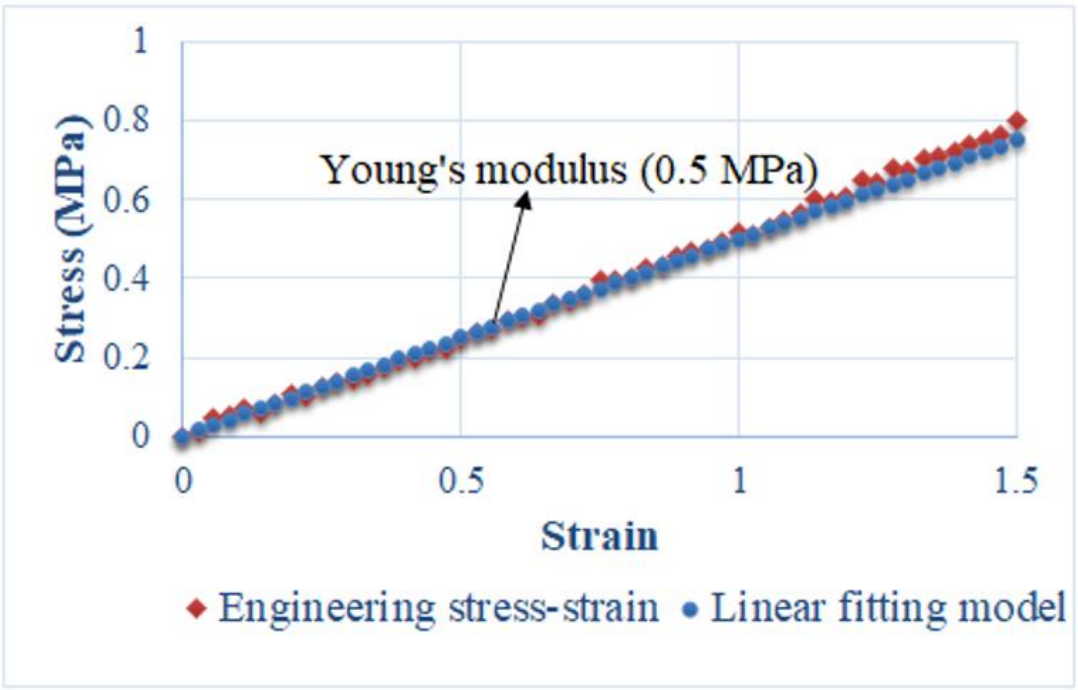

(b)

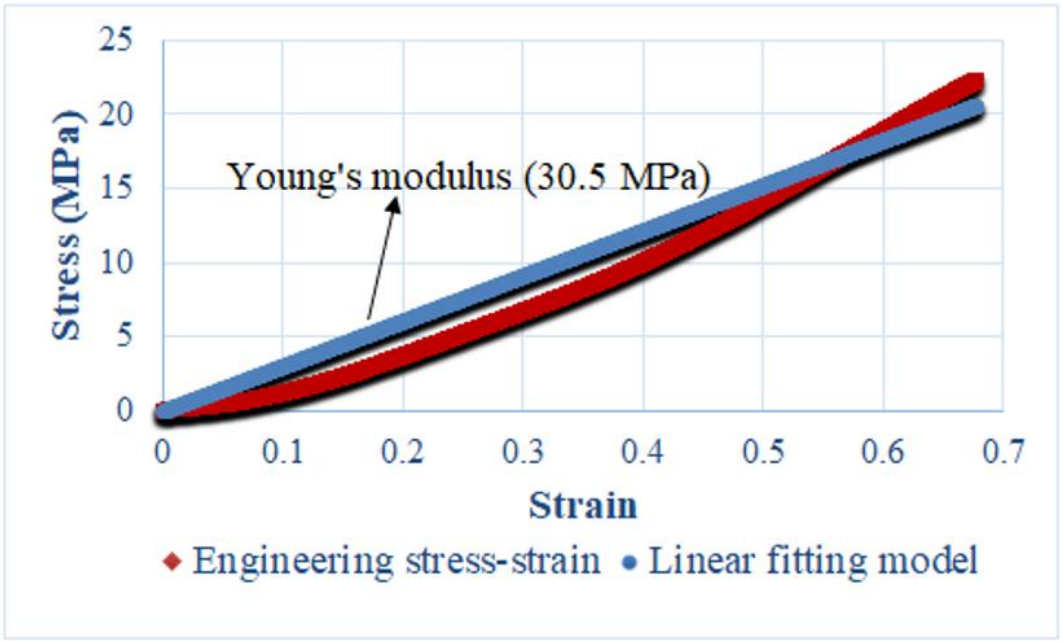

(c)

Figure 4 Proposed materials' models based on the experimental results: (a) stiff underlaps; (b) elastic underlaps; (c) wales.

Finite element models and boundary conditions

Based on the geometrical model of one basic unit, the finite element models loading in the wale direction (y direction) and course direction (x direction) were established as shown in Figure 5 (a) and Figure 5 (b), respectively. Then, the models were imported into ANSYS/LS-DYNA for analysis and the respective materials and their properties would be assigned to each component. In order to simulate the deformation of the fabric structure under tension, two stiff guide plates were introduced to both ends of the models to facilitate the application of tensile load, as shown in Figure 5. Rigid model was used for the plates. Their Young's modulus was set as 2500MPa. Element type of Solid164 was adopted and the tetrahedral mesh scheme was used to mesh the wales, underlaps and the two stiff guide plates. The mesh size for the stiff underlaps, elastic underlaps and the wales is 0.5mm, 0.07mm and 0.07mm, respectively.

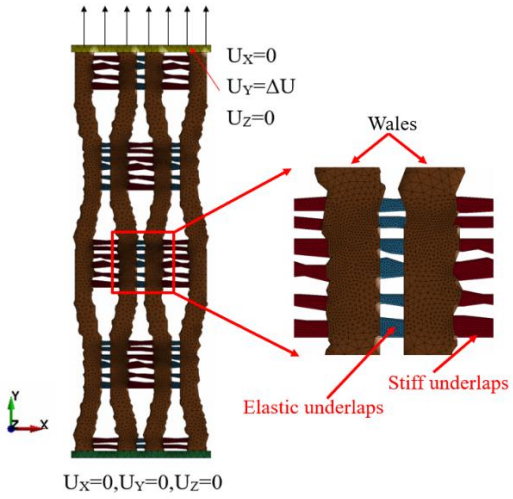

(a)

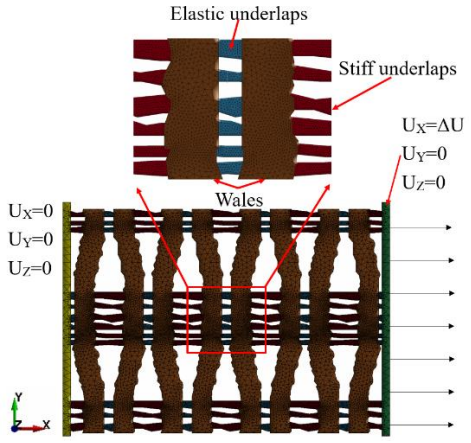

(b)

Figure 5 Finite element models: (a) loading in wale direction (y- direction); (b) loading in course direction (x- direction).

The boundary conditions in the wale and course tensile directions were applied to simulate the real tensile experiments. As there are no out-of-plane loading in the tests, only translational degrees of freedom are exerted on the models. As shown in Figure 5, for the model in the wale direction (y direction), y- directional tension loading is exerted with the bottom stiff plate fixed and the upper plate stretched. Therefore, the boundary conditions for the bottom plate are $U_X=U_Y=U_Z=0$, while for the upper plate the boundary conditions are $U_X=0$ and $U_Y = \Delta U$ where ΔU is the tensile displacement. For the model in the course direction (x direction), x- directional tension loading was exerted with the left stiff plate fixed and the right plate stretched. The boundary conditions for left plate were $U_X=U_Y=U_Z=0$, while for the right plate the boundary conditions are $U_Y=0$ and $U_X= \Delta U$ where ΔU is the tensile displacement.

Calculation of Poisson's ratio

After the simulation, Poisson's ratio was calculated by using the post-processor, LS-PrePost. The displacement of each node in the structure could be readily recorded. As shown in Figure 6 (a), in y- directional loading, deformation in tensile direction was measured 5 times near points W_1 and W_2 to calculate the average displacement of the tensile strain while deformation in lateral direction was measured 5 times near points W_3 and W_4 to calculate the average displacement of the lateral strain. In the case of x-directional loading, as shown in Figure 6 (b), similarly, lateral deformation was

measured 5 times near points C_1 and C_2 to calculate the average displacement of the lateral strain while deformation in tensile direction was measured 5 times near points points C_3 and C_4 to calculate the average displacement of the tensile strain. Then Poisson's ratio v could be calculated from Equation (1).

$$v = -\frac{\varepsilon_l}{\varepsilon_t} \quad (1)$$

Where ε_l and ε_t are the lateral strain and tensile strain, respectively.

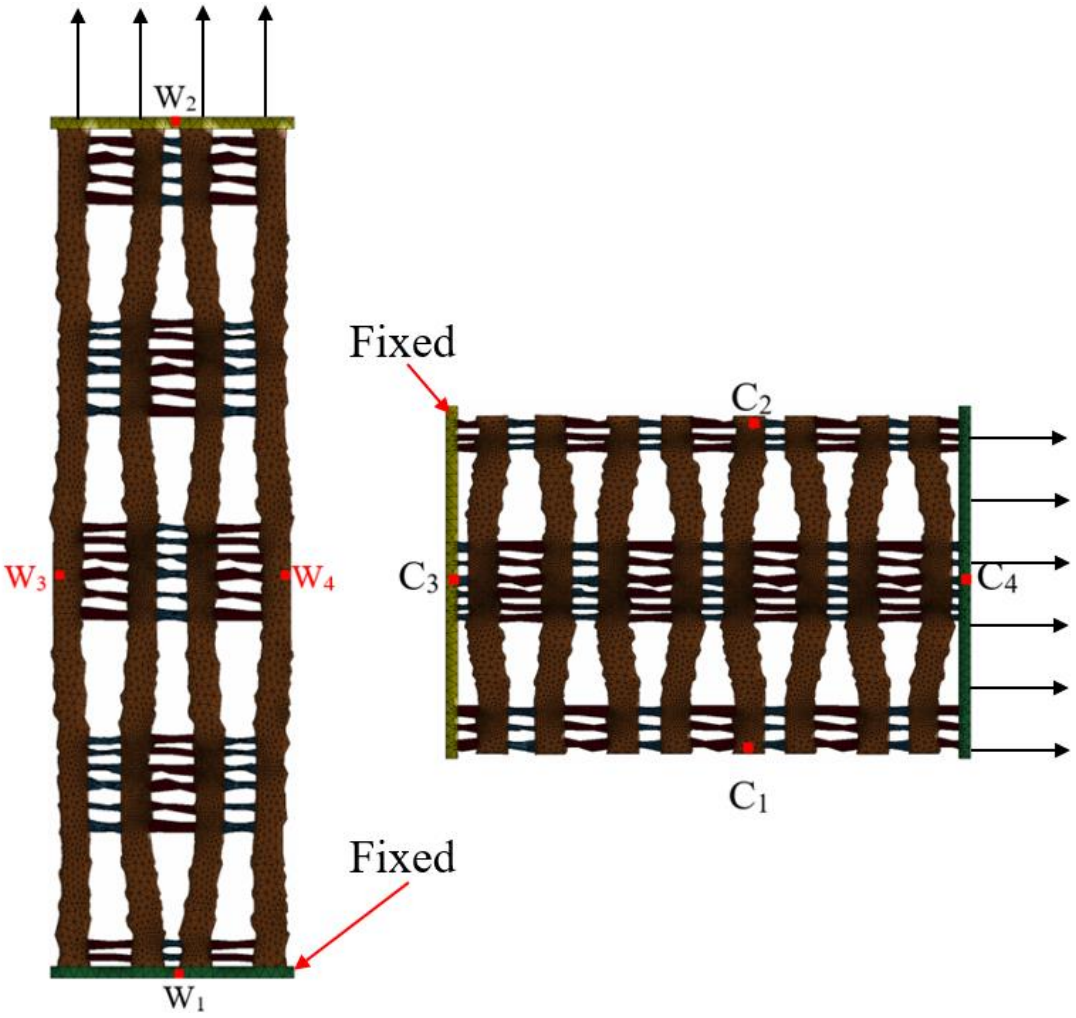

(a) (b)

Figure 6 Calculation of Poisson's ratio: (a) loading in wale direction (y- direction); (b) loading in course direction (x- direction).

To verify the models, Poisson's ratio values obtained from the experiments were used for comparison. As presented in our previous research [14], the experiments were conducted on an Instron 5566 tensile machine. Samples were cut with a standard size of 250 mm in length and 50 mm in width. The gauge length was set as 150 mm. Before the tests, points were marked on the samples. The tensile speed was set as 50 mm/min. For the samples in each direction, three tests were conducted, and average Poisson's ratio values were calculated after the tests.

Results and discussion

Fabric deformations at different tensile strains

Figure 7 shows the simulated deformations of the auxetic warp knitted fabric structure at different tensile strains when loaded in the wale direction. To verify the simulation, the deformations of the real fabric at the same tensile strains were also shown for comparison. It can be seen that the simulated deformations from the model are similar to the experimental deformations. With the elongation in the wale direction, diagonal ribs in both the model and real fabric tend to turn to the wale direction causing the expanding of elastic underlaps. As a result, the lateral size of the model as well as the real fabric increases. However, the diagonal ribs in the model cannot rotate freely because they are considered as continuous isotropic elastic materials. The elongation of

the model only achieved 20%. While in the deformation of the real fabric, the extension could be much larger, because the diagonal ribs are easy to extend and rotate due to the deformation of loops and transformation of yarns.

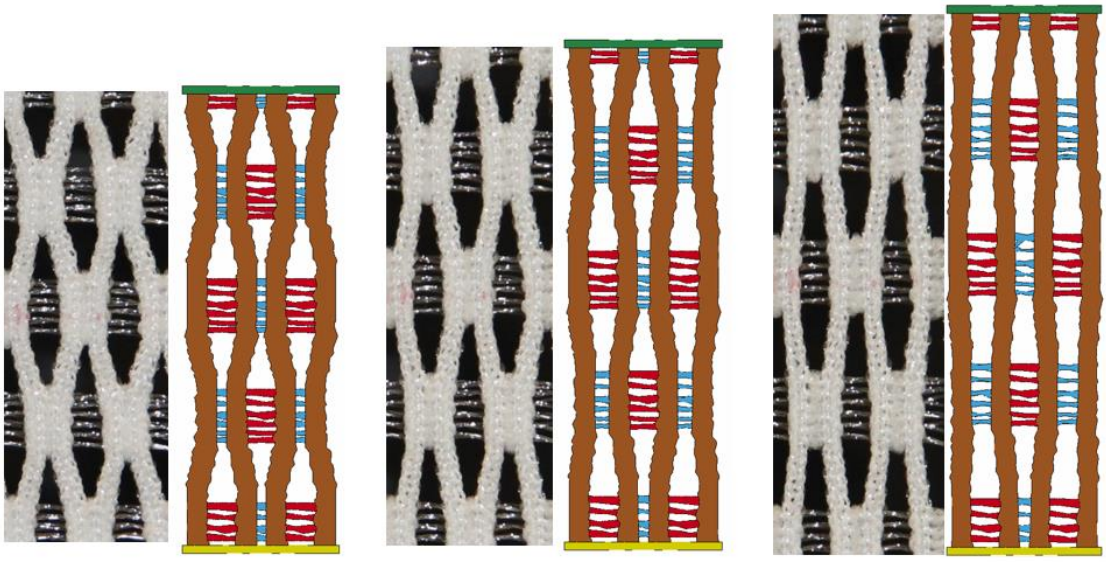

(a) (b) (c)

Figure 7 Deformations of simulation and real fabric at different tensile strains when loaded in wale direction: (a) 0%; (b) 10%; (c) 20%.

The deformations of the model and real fabric when loaded in the course direction are shown in Figure 8. It can be seen that with the increase of tensile strain, elastic underlaps in both the model and real fabric are extended which cause the rotation of diagonal ribs. As a result, the lateral size is increased and auxetic effect is obtained. It can also be observed that the deformations under tension in the model are similar to those of the real fabric, although the deformations in the real fabric are more distinctive. The differences are caused by the fact that the model was simplified and not established at

yarn level. On the other hand, the materials in the model were considered as continuous isotropic materials. Therefore, the rotation of the wales and extension of elastic underlaps in the model were limited, and the model could only be used to predict the deformations of the fabric below 10% of the tensile strain.

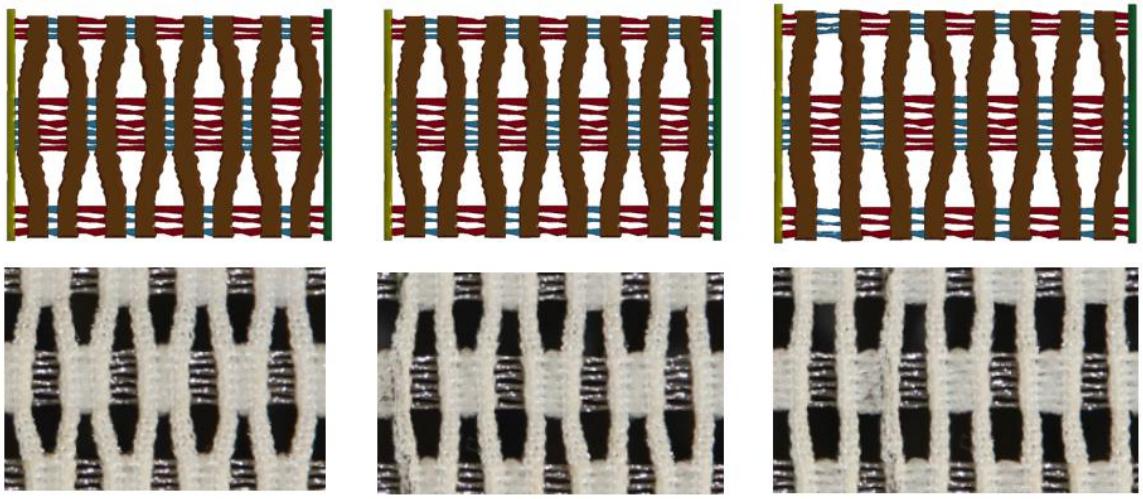

(a) (b) (c)

Figure 8 Deformations of model and real fabric at different tensile strains when loaded in course direction: (a) 0%; (b) 4%; (c) 10%.

Poisson's ratio

Poisson's ratio variations from both simulation and experiment as a function of tensile strain when stretched in the wale direction and course direction are shown in Figure 9 and Figure 10, respectively. It can be found that the simulated results have the same trends as the experimental ones in both directions. In case of loading in the wale direction, it can be seen from Figure 9 that Poisson's ratio first decreases and then

increases. The minimum Poisson's ratio simulated is fallen between 10% and 15% of tensile strain, which is the same as the experimental results. Although the auxetic effect of the simulation is slightly lower than that of the real fabric, the simulated results are approximate to the experimental ones. With tensile strain changing from 2% to 12%, Poisson's ratio of the simulation varies from -0.23 to -0.38, while the experimental result varies from -0.25 to -0.46. With tensile strain increasing to 20%, Poisson's ratio of the simulation reaches -0.29, while Poisson's ratio from the experiments approaches -0.42. The maximum difference in auxetic effect between simulation and experiment does not exceed 30%.

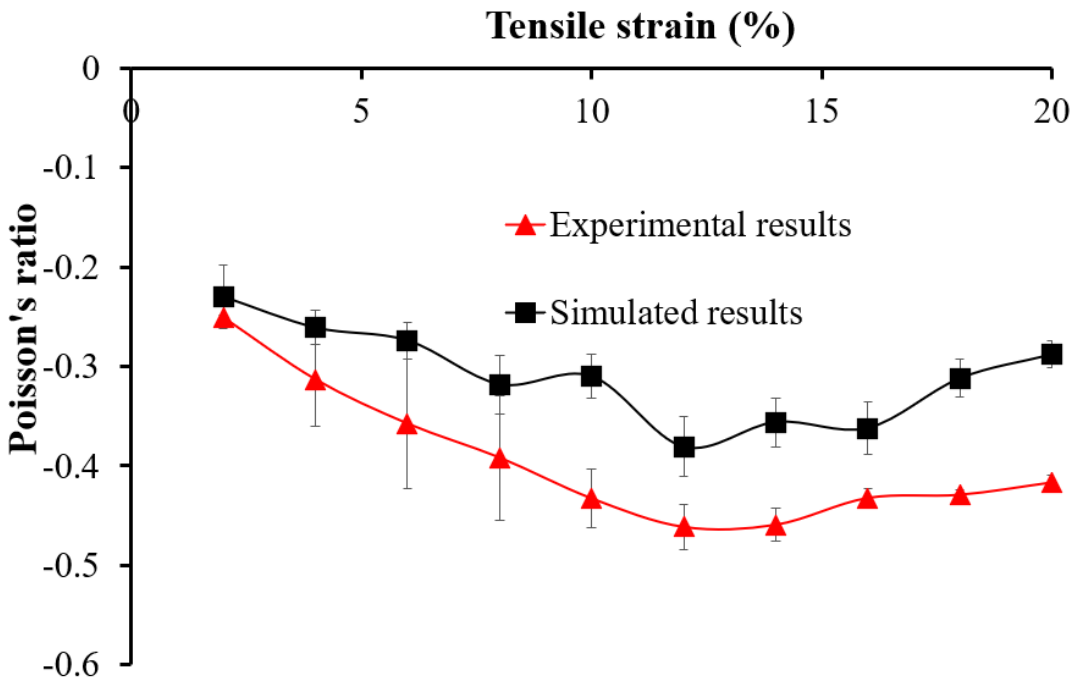

Figure 9 Comparison of Poisson's ratio between simulation and experiment when loaded in wale direction.

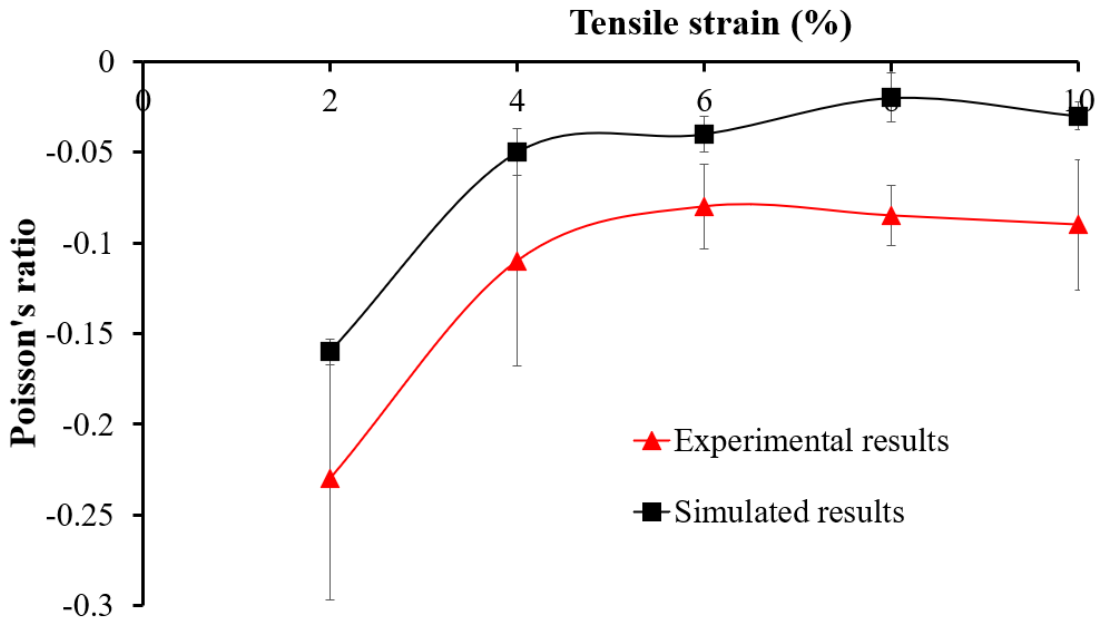

Figure 10 Comparison of Poisson's ratio between simulation and experiment when loaded in course direction.

In case of loading in the course direction, it can be seen from Figure 10 that Poisson's ratio of both simulation and real fabric firstly increases and then tends to be stablized with the increase of the tensile strain. Being the same as loading in the wale direction, the auxteic effect of the simulation in this case is also lower than that of the real fabric. At tensile strain 2%, Poisson's ratio from experiment is approximate to -0.25 while that of the simulation is -0.16. When tensile strain exceeds 6%, Poisson's ratio from experiments tends to be stabilized at 0. 1 while that from the simulation fluactuates around 0.05.

The differences between the simulation and experiments in two direction mainly come from the simplification of the models because the wales of fabric structure were simplified as continuous materials which could not rotate freely as the wales in real

fabric. In addition, yarn slippage effect could not be taken into consideration in the finite element models. However, since the simulated results in both wale direction and course direction exhibit similar variation trends as experimental ones, the established models could be used to predict auxetic behavior of real fabric. As the differences between the models and real fabric lies in the simplification of the models, more accurate results can be achieved by using the models based on yarn level.

Conclusions

Finite element models of the reentrant fabric structure in both wale direction and course direction were established and analyzed using UG 10.0 and ANSYS/LS-DYNA 16.0. And the LS-PrePost was used to calculate Poisson's ratio of the simulated fabric structure. Finally, deformations and Poisson's ratio were compared between the simulation and experiment. From this work, the following conclusions can be achieved:

(1) The models established can be used to predict auxetic behavior of the fabric. However, the simulation can only be used for prediction within a smaller range of tensile strains. Posson's ratio values from the simulation are generally higher than those of the experiments with an acceptable deviation. However, their variation trends agree well between the simulation and experiment.

(2) More precise results can be achived by establishing a model with a smaller mesh size at yarn level to narrow the difference between simulation and experiment. However,

the time consumed for simulation will also increase, so that a balance between efficiency and accuracy should be made.

This research is focused on a finite element simulation of auxetic warp knitted fabric structure. Although the models proposed can be used to predict auxetic effect of the real fabric, the accurcy still needs to be improved. In addition, the models are only established based on one fabric structure, influences of geometrical parameters like rib and underlap lengths on auxetic effect are still not simulated. Therefore, future work can be continued in the optimization of the finite element simulation to make it more accurate. At the same time, effects of different geometrical parameters will be included in the simulation.

Acknowledgements

The authors would like to thank the funding support from the Research Grants Council of Hong Kong Special Administrative Region Government for the GRF project (grant number: 15209616).

Reference

1. Ma, P., et al., *Review on the knitted structures with auxetic effect.* The Journal of The Textile Institute, 2017. **108**(6): p. 947-961.
2. Hu, H. and A. Zulifqar, *Auxetic textile materials-a review.* J Text Eng Fashion Technol, 2016. **1**(1): p. 00002.
3. Liu, Y. and H. Hu, *A review on auxetic structures and polymeric materials.* Scientific Research and Essays, 2010. **5**(10): p. 1052-1063.

4. Wang, Z. and H. Hu, *Auxetic materials and their potential applications in textiles.* Textile Research Journal, 2014. **84**(15): p. 1600-1611.
5. Hu, H., M. Zhang, and Y. Liu, *Auxetic textiles*. 2019: Woodhead Publishing.
6. Cao, H., et al., *Bi-stretch auxetic woven fabrics based on foldable geometry.* Textile Research Journal, 2019. **89**(13): p. 2694-2712.
7. Zulifqar, A. and H. Hu, *Development of bi-stretch auxetic woven fabrics based on re-entrant hexagonal geometry.* physica status solidi (b), 2019. **256**(1): p. 1800172.
8. Zulifqar, A., T. Hua, and H. Hu, *Single-and Double-Layered Bistretch Auxetic Woven Fabrics Made of Nonauxetic Yarns Based on Foldable Geometries.* physica status solidi (b), 2020. **257**(10): p. 1900156.
9. Ng, W.S. and H. Hu, *Woven fabrics made of auxetic plied yarns.* Polymers, 2018. **10**(2): p. 226.
10. Gao, Y., et al., *Manufacture and evaluation of auxetic yarns and woven fabrics*. physica status solidi (b), 2020. **257**(10): p. 1900112.
11. Liaqat, M., et al., *The development of novel auxetic woven structure for impact applications.* The Journal of the Textile Institute, 2017. **108**(7): p. 1264-1270.
12. Chen, J., Z. Du, and T. Li, *Structural design and characterization of highly elastic woven fabric containing helical auxetic yarns.* Textile Research Journal, 2020. **90**(7-8): p. 809-823.

13. Hu, H., Z. Wang, and S. Liu, *Development of auxetic fabrics using flat knitting technology.* Textile Research Journal, 2011. **81**(14): p. 1493-1502.

14. Zhao, S., et al., *Development of auxetic warp knitted fabrics based on reentrant geometry.* Textile Research Journal, 2020. **90**(3-4): p. 344-356.

15. Wang, Z. and H. Hu, *3 D auxetic warp-knitted spacer fabrics.* physica status solidi (b), 2014. **251**(2): p. 281-288.

16. Uzun, M. and I. Patel, *Tribological properties of auxetic and conventional polypropylene weft knitted fabrics.* Archives of Materials Science and Engineering, 2010. **44**(2): p. 120-125.

17. Alderson, K., et al., *Auxetic warp knit textile structures.* physica status solidi (b), 2012. **249**(7): p. 1322-1329.

18. Ma, P., Y. Chang, and G. Jiang, *Design and fabrication of auxetic warp-knitted structures with a rotational hexagonal loop.* Textile Research Journal, 2016. **86**(20): p. 2151-2157.

19. Verma, P., et al., *Inducing out-of-plane auxetic behavior in needle-punched nonwovens.* physica status solidi (b), 2015. **252**(7): p. 1455-1464.

20. Verma, P., et al., *Induction of auxetic response in needle-punched nonwovens: Effects of temperature, pressure, and time.* physica status solidi (b), 2016. **253**(7): p. 1270-1278.

21. Verma, P., et al., *Wool nonwovens as candidates for commodity auxetic materials.* Engineering Research Express, 2020. **2**(4): p. 045034.

22. Ge, Z. and H. Hu, *Innovative three-dimensional fabric structure with negative Poisson's ratio for composite reinforcement.* Textile Research Journal, 2013. **83**(5): p. 543-550.

23. Liu, Y., et al., *Negative Poisson's ratio weft-knitted fabrics.* Textile Research Journal, 2010. **80**(9): p. 856-863.

24. Glazzard, M. and P. Breedon, *Weft-knitted auxetic textile design.* physica status solidi (b), 2014. **251**(2): p. 267-272.

25. Boakye, A., et al., *Design and manufacture of knitted tubular fabric with auxetic effect.* The Journal of The Textile Institute, 2018. **109**(5): p. 596-602.

26. Xu, W., et al., *Design and fabrication of novel auxetic weft-knitted fabrics with Kevlar yarns.* The Journal of The Textile Institute, 2018.

27. Ugbolue, S.C., et al., *The formation and performance of auxetic textiles. Part II: geometry and structural properties.* The Journal of the Textile Institute, 2011. **102**(5): p. 424-433.

28. Lim, T.-C., *Negative hygrothermal expansion of reinforced double arrowhead microstructure.* physica status solidi (b), 2020. **257**(10): p. 1800055.

29. Chang, Y. and P. Ma, *Fabrication and property of auxetic warp-knitted spacer structures with mesh.* Textile Research Journal, 2018. **88**(19): p. 2206-2213.

30. Shuaiquan, Z., et al., *Auxetic behavior of warp knitted fabric under repeating tension.* Textile Research Journal, 2021: p. 0040517521989277.